5th US Combustion Meeting
Organized by the Western States Section of the Combustion Institute
and Hosted by the University of California at San Diego
March 25-28, 2007.

Direct numerical simulation of transient ignition of diluted hydrogen versus heated air in axisymmetric counterflow

Chun Sang Yoo, Jacqueline H. Chen, and Jonathan H. Frank

Combustion Research Facility, Sandia National Laboratories
7011 East Ave., Livermore, California 94551-0969, USA

The sensitivity of super-equilibrium OH to the initial width and amplitude of O-atom deposition used to trigger ignition in a mixing layer of heated air versus ambient hydrogen/nitrogen is numerically investigated in an axisymmetric counterflow configuration. This represents an extension of a previous study that compared one-dimensional opposed jet computations with an axisymmetric counterflow ignition experiment. The previous one-dimensional computations did not capture the degree of super-equilibrium OH that was measured during the transition from thermal runaway to the formation of a steady flame. The present two-dimensional simulations show that the spatial distribution and the magnitude of the OH overshoot are governed by multi-dimensional effects. The degree of OH overshoot increases as the diameter of the initial O-atom deposition region decreases. This result is attributed to preferential diffusion of hydrogen in the highly curved leading portion of the edge flame that is established following thermal runaway at the ignition kernel. The simulations show that the ignition delay decreases as the amplitude of the initial O-atom deposition increases as expected. It is also found that the structure of the resulting diffusion flame corresponds to Liñán's 'premixed flame regime' in which only the oxidizer leaks through the reaction zone. The flame exists under fuel lean rather than stoichiometric mixture fraction conditions. The edge flame structure resulting from thermal runaway in the present nonpremixed counterflow system resembles edge flames in a homogenous mixture flowing against hot inert in counterflow.

1. Introduction

Ignition and subsequent edge flame formation are important processes that occur in many practical combustion systems characterized by turbulence intermittency as well as finite-rate chemistry. Better understanding of these fundamental processes is critical to the design and operation of combustion systems, and hence, they have been widely studied. Models have attempted to characterize these processes in terms of a few relevant parameters, such as scalar dissipation rate and mixture fraction.

Theoretical studies of autoignition in steady and unsteady nonpremixed systems using one-step chemistry have established ignition criteria in terms of Damköhler and reactant Lewis numbers [1–4]. In many experimental and numerical studies, finite-rate chemistry was adopted to investigate the effects of pressure, flow strain, heating, and chemical additives on ignition limits and delay times [5–9]. Transient autoignition with oscillatory strain conditions was studied with one-dimensional counterflow calculations to better understand ignition in turbulent flows [10–12]. In addition, direct numerical simulations (DNS) have been performed to characterize the

effect of turbulence-chemistry interactions on autoignition and subsequent combustion process [13–15].

Edge flames have also been widely studied because of their relevance to the stabilization mechanism of turbulent lifted flames, flame spread over a fuel bed, and autoignition. Theoretical and numerical studies with one-step chemistry have investigated the edge flame speed and instability in counterflows [16–20]. The characteristics of edge flame propagation have also been determined by DNS with detailed chemistry [21–26].

Accurate modeling of combustion processes requires a fundamental understanding of the transient nature of autoignition in nonuniform flows. In a previous study [9], the transient characteristics of ignition of hydrogen diluted by nitrogen versus heated air in an axisymmetric counterflow were studied both experimentally and numerically. In the experiments, a high degree of OH overshoot was observed during ignition. However, one-dimensional computations did not capture the degree of OH overshoot that was measured in the experiments and it was hypothesized that multi-dimensional effects on edge flames may account for the discrepancy between the computation and experiment. In the present work, we study the multi-dimensional effects on ignition characteristics using axisymmetric direct numerical simulations of the ignition of hydrogen versus heated air with detailed hydrogen/air chemistry and mixture averaged-transport properties. In the following, we examine the ignition characteristics of the flow and the degree of OH overshoot and investigate the structure of the nonpremixed flame that is established after ignition. Finally, we discuss the topology of the edge flame which develops after thermal runaway at the ignition kernel.

2. Numerical methods

Direct numerical simulations of transient ignition of hydrogen diluted with nitrogen against heated air are performed in an axisymmetric counterflow configuration. Using the DNS code, S3D, the compressible Navier-Stokes, species continuity, and total energy equations are solved with a fourth-order explicit Runge-Kutta method for time integration and an eighth-order central spatial differencing scheme [27, 28]. A tenth-order filter is used to remove any spurious high-wave number oscillations. To simulate ignition in the axisymmetric counterflow efficiently, S3D utilizes a two-dimensional cylindrical coordinate system using the method proposed by Mohseni and Colonius [29], whereby polar grid points are removed from the grid system and thus, singularity at the pole is avoided. A detailed hydrogen/air kinetic mechanism [30] is used and CHEMKIN software libraries [31] are linked with S3D to evaluate reaction rates, thermodynamic and mixture-averaged transport properties.

Figure 1 shows the initial conditions for the ignition simulations. The domain size is $L_x \times R = 1.2$ cm $\times$ 1.2 cm, with 400 grid points in each direction. Following the previous study [9], the inlet temperatures and species mole fractions are given as $T_1 = 298$ K, $X_{H2,1} = 0.08$, $X_{N2,1} = 0.92$, and $T_2 = 946$ K, $X_{O2,2} = 0.21$, $X_{N2,2} = 0.79$, where subscripts 1 and 2 denote fuel and oxidizer streams, respectively. The inlet flows are assumed to be plug flow and axial velocities are specified as $V_{x,1} = 53.13$ cm/s and $V_{x,2} = 90$ cm/s such that the overall strain rate based on the oxidizer stream is given by $a_2 = 300$ s^{-1} [32]. Used are improved nonreflecting inflow/outflow boundary conditions which were previously developed and implemented in S3D for reacting counterflow simulations [23, 33–35]. Symmetry conditions are specified at the polar axis. With the

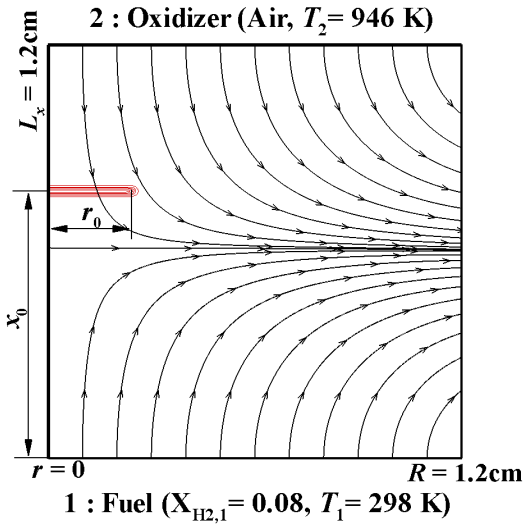

Figure 1: Initial conditions for transient ignition in axisymmetric counterflow. Solid and arrowed lines represent the initial profile of the O-atom deposition and streamlines of the counterflow, respectively.

conditions, a steady hydrogen/air nonpremixed counterflow flame was established, where the streamlines of the steady flow are shown in Fig. 1.

To initiate the ignition, we simulate the laser-triggered ignition in our previous experimental study [9]. In the experiments, ignition was initiated with a pulsed laser that photodissociated molecular oxygen in the heated air flow to form a sheet of O(^{3}P) atoms. For the simulations, we introduce oxygen atoms in a disk-shaped region that is centered on the burner axis at x_0 = 7.75 mm. The initial profile of the O-atom mole fraction, X_O, is specified as:

$$X_O = X_{O,max} \exp\left[-\frac{(x-x_0)^2}{2\sigma^2}\right] \cdot \frac{1}{2}\left[1-\tanh\left(\frac{r-r_0}{\delta}\right)\right], \quad (1)$$

where r_0 represents the half width of the laser beam, $X_{O,max}$ the maximum oxygen atom mole fraction, σ = 0.075 mm, and δ = 0.1 mm. The solid lines in the oxidizer stream in Fig. 1 represent the isocontours of the initial O-atom deposition.

3. Multi-dimensional and initial condition effects on the degree of OH overshoot

In the previous study [9], one-dimensional opposed jet calculations predicted super-equilibrium OH mole fraction, $X_{OH,}$ following thermal runaway and preceding the establishment of a steady flame. However, the one-dimensional results underestimated the degree of OH overshoot by 40% compared to the experiment. This discrepancy in the degree of OH overshoot between one-dimensional simulations and experiments has been conjectured to be due to multi-dimensional effects such as preferential diffusion of hydrogen into a highly curved edge flame [21, 22], and the decrease of strain rate due to flow divergence ahead of the edge flame. In this section, multi-dimensional effects on the degree of OH overshoot and the sensitivity of OH overshoot to the initial width and amplitude of O-atom deposition are examined.

Table 1. The maximum mole fraction and width of the O-atom deposition for Cases 1-6.

Case	$X_{O,max}$	r_0 [mm]
1	0.0013	∞
2	0.0013	2.5
3	0.0013	2.0
4	0.0013	1.5
5	0.00195	2.5
6	0.000975	2.5

3.1. Multi-dimensional effects

To investigate the multi-dimensional effects on the degree of OH overshoot, first an unsteady DNS of ignition in axisymmetric counterflow is performed with the same initial conditions ($X_{O,max}$ = 0.0013 and r_0 = 2.5 mm) as used in Ref. [9] and given as Case 2 in Table 1. Figure 2 shows consecutive images of (a) the OH LIF signal from the experiments and (b) OH mole fraction, X_{OH} from the simulation. The OH LIF signals were corrected for variations in the laser beam profile. For the majority of the sequence in Fig. 2, the OH LIF signal provides an accurate measure of the variations in the OH mole fraction without any corrections for variations in

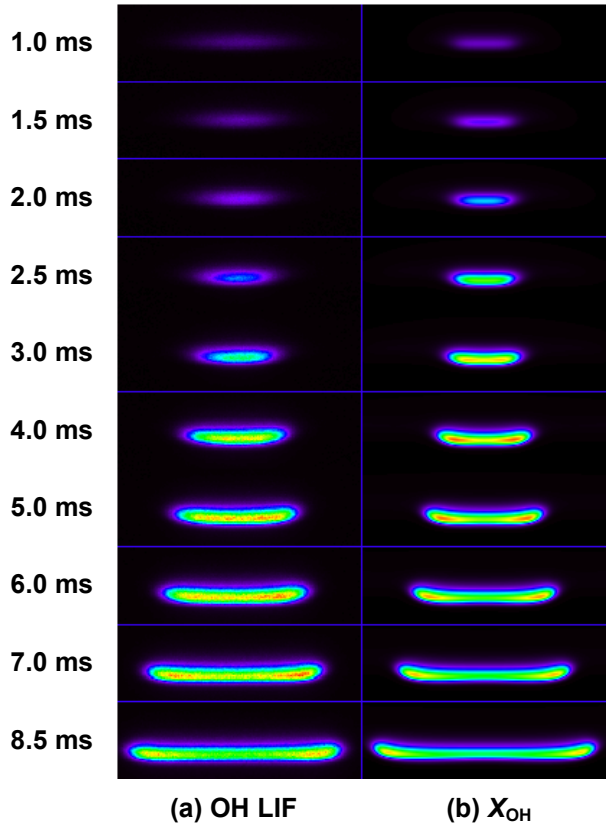

Figure 2: Temporal evolution of (a) OH LIF signal in the experiment and (b) OH mole fraction in the simulation.

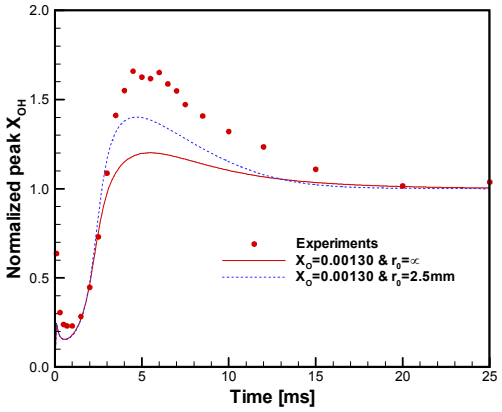

Figure 3: Comparison of measured and computed temporal evolution of the peak centerline OH mole fraction during the ignition of a nonpremixed counterflow of N_2-diluted H_2 and heated air. The OH mole fraction is normalized with respect to the corresponding value in the steady state flame.

collisional quenching rates and Boltzmann fraction [9]. The simulation shows good agreement with the experimental results in terms of the edge location and the overall shape of the edge flame. The OH mole fraction at the edge flame increases while the edge flame is developing, but after a steadily propagating edge flame is established, its peak OH mole fraction remains constant until it propagates out of the domain. The peak OH mole fraction is located near the tip of the edge flame, and the super-equilibrium OH extends into the diffusion flame. Thus, it is reasonable to consider that the OH overshoot in the diffusion flame is affected by the OH increase in the edge flame

To quantify the degree of OH overshoot, we integrate the OH mole fraction and OH LIF signals over a 2.8 mm wide region that is centered on the ignition kernel, following the analysis in Ref. [9]. Figure 3 compares the computed and measured temporal evolution of the peak OH mole fraction along the burner centerline. In addition to simulating Case 2, we include results from Case 1 with $r_0 = \infty$, which emulates a one-dimensional simulation in a two-dimensional axisymmetric domain. The integrated values are normalized by the corresponding value in the steady flame. For Case 1, the degree of OH overshoot is approximately 20 % as predicted by the one-dimensional simulations [9]. For the Case 2, however, the centerline peak X_{OH} overshoots the steady-flame value by 40 % and then decreases gradually as the edge flame propagates out of the domain. A comparison of the axisymmetric and one-dimensional simulations clearly shows the significance of multi-dimensional effects on the degree of OH overshoot. The discrepancy in the OH overshoot between experiment and computation is reduced by accounting for multi-dimensional effects. The remaining discrepancy may result from slight differences between the velocity and temperature profiles in the experiments and simulations. In addition, asymmetries that are introduced into the initial O-atom distribution by the intersection of the laser sheet with the axisymmetric counterflow are not accounted for in the simulation.

The multi-dimensional effect is a result of preferential diffusion of hydrogen at the highly curved edge flame which results in enhanced production of the hydroxyl radical. This mechanism for the enhanced OH overshoot in the axisymmetric simulation is better understood by examining the maximum X_{OH} and hydrogen diffusive flux in the edge flame presented in Fig. 4. In Fig. 4(a) the maximum X_{OH} at the edge flame increases to 1.6 times its value in the steady diffusion flame

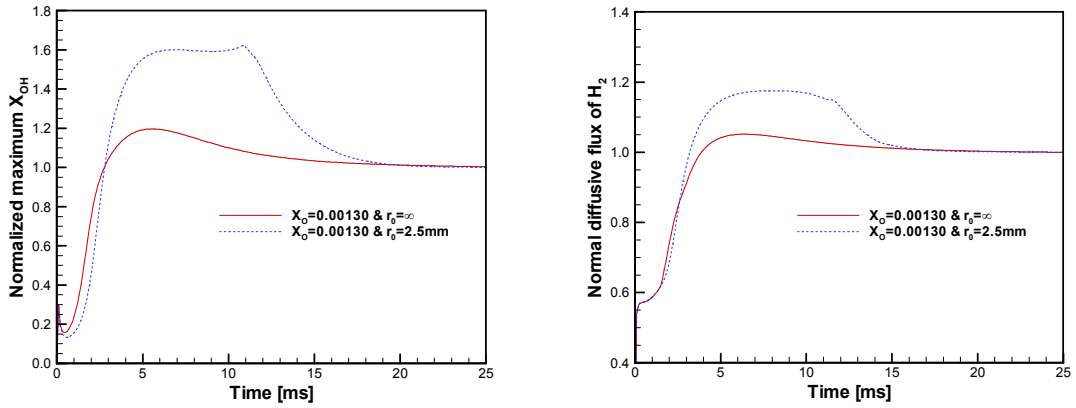

(a) Maximum X_{OH} **(b) Normal diffusive flux of H_2**

Figure 4: Temporal evolution of (a) the maximum $X_{OH,}$ and (b) the normal diffusive flux of H_2 into the flame.

and remains nearly constant in time until the edge flame passes through the boundary at 11 ms. The perturbation in Fig. 4(a) at 11 ms is an artifact of the edge flame passing through the domain boundary. Similarly, the maximum hydrogen diffusive flux into the edge flame is enhanced by up to 1.18 times its value in the steady nonpremixed flame as shown in Fig. 4(b). The higher diffusive flux into the flame enhances chemical reaction and thus, one can expect the OH overshoot. These results along with the simulation images in Fig. 2 confirm that the degree of OH overshoot is enhanced by the intensification of OH at the edge flame due to preferential diffusion of hydrogen into the edge flame. Moreover, if the radial extent of the ignition kernel is small and comparable to the curvature of the edge flame, then the degree of OH overshoot is further amplified. This issue will be investigated in the next section.

In the previous study [9], it was hypothesized that the decrease of strain rate due to flow divergence in the leading portion of the edge flame could result in the OH overshoot. However, there is no clear evidence showing flow divergence at the leading edge of the flame during the simulation. This may be attributed to the weakness of the highly diluted flame to significantly alter the flow and strain rate. Thus, preferential diffusion of hydrogen is identified as the main source of the degree of OH overshoot.

3.2. Ignition sensitivity to structure and amplitude of initial O-atom deposition

The sensitivity of the temporal development of the ignition kernel and subsequent edge flame formation and propagation to the structure of the initial O-atom deposition used to trigger ignition is investigated. In particular, the effects of the initial width and maximum amplitude of the O-atom deposition on the ignition delay and extent of OH overshoot are examined in a set of axisymmetric simulations given in Table 1.

The effect of the initial width of O-atom deposition on the evolution of ignition characteristics is presented in Fig. 5 for (a) the peak centerline values of X_{OH} and (b) the maximum X_{OH} in the computational domain. All values are normalized by the corresponding values in the steady flame. In Fig. 5 (a), note that as the width of the O-atom deposition decreases, the degree of OH overshoot increases from 20 % in Case 1 to over 90 % in Case 4. The increase in the degree of OH overshoot is attributed to the location of the edge flame following thermal runaway.

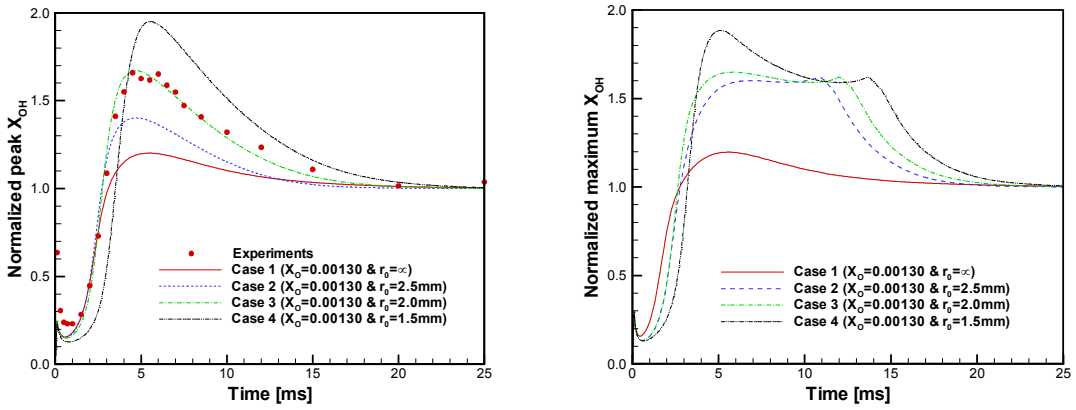

(a) Peak centerline X_{OH} **(b) Maximum X_{OH}**

Figure 5: Temporal evolution of (a) peak centerline X_{OH} and (b) maximum X_{OH} for Cases 1-4.

As the width of the O-atom deposition decreases, the size of the corresponding flame established after thermal runaway becomes smaller such that the curvature of the radial flame becomes large and comparable to the curvature of the leading edge of the flame. Therefore, both curvatures additively induce significant preferential diffusion of hydrogen into the flame. However, this initial O-atom width effect diminishes as the radial extent of the flame increases in time, such that ultimately, the shape of the leading edge becomes the dominant curvature effect. Figure 5(b) clearly shows the result of preferential diffusion by the curvature of the flame. As the size of the O-atom deposition decreases, the degree of overshoot of maximum X_{OH} increases significantly, similar to that of the peak centerline X_{OH}. Therefore, the influence of the initial O-atom width increases as the size of the deposition decreases. Note that the maximum X_{OH} coincides with the leading edge of the flame so that the global maximum X_{OH} coincides with the maximum X_{OH} at the edge flame.

Next, the sensitivity of the degree of OH overshoot and ignition delay to the amplitude of the O-atom deposition is examined. Figure 6 shows the temporal evolutions of (a) peak centerline X_{OH} and (b) maximum X_{OH} through the domain for Cases 2, 5 and 6 in Table 1. Both the peak

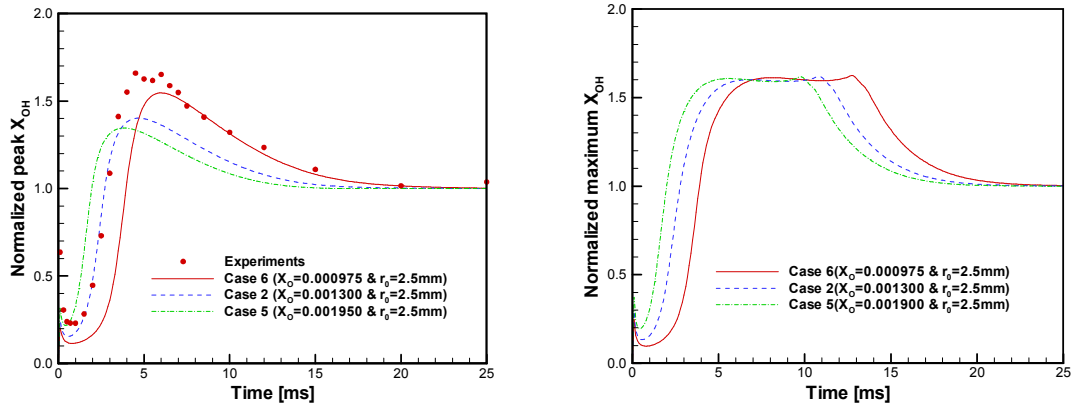

(a) Peak centerline X_{OH} **(b) Maximum X_{OH}**

Figure 6: Temporal evolution of (a) peak centerline X_{OH} and (b) maximum X_{OH} for Cases 2, 5, and 6.

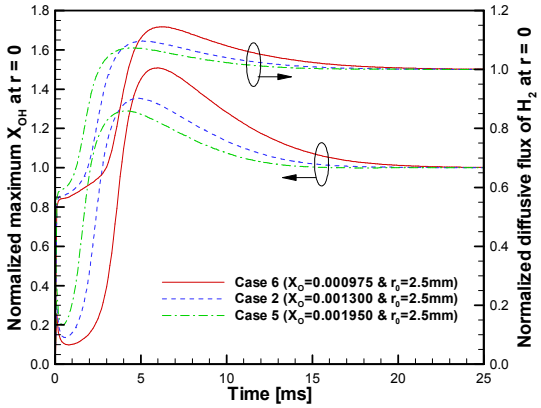

Figure 7: Temporal evolution of the maximum X_{OH} and hydrogen diffusive flux at the centerline for Cases 2, 5, and 6.

centerline X_{OH} as well as the ignition delay increase as the maximum amplitude of O-atom deposition decreases. However, the maximum X_{OH} in the Fig. 6(b) is the same for all of the cases, but is shifted by a time lag due to differences in ignition delay. As expected, the ignition delay is reduced for larger deposition of O-atom due to enhanced chemical reaction during the early induction stage of ignition. A constant value of maximum X_{OH} is attained with different O-atom depositions because edge flames are generated at a similar location and thus, the history of their development should be similar.

On the contrary, the peak centerline X_{OH} value shows an increasing trend with decreasing O-atom deposition. This is because an ignition kernel with a small amplitude X_O requires a longer induction time to build up a radical pool sufficient for thermal runaway. As a result, the traces of the edge flame in the central 2.8 mm integration window remain longer even after the edge flame propagates out of this window. Thus, the peak centerline X_{OH} increases even though fully developed edge flames have identical maximum X_{OH} and structure. These traces associated with the edge formation can be found in the temporal variation of the maximum X_{OH} and hydrogen diffusive flux into the flame at the centerline as shown in Fig. 7. Even if the diffusive flux in Case 6 grows slowly compared to other cases, its peak is much higher and lasts longer than the others. As a result, the higher diffusive flux induces a higher degree of OH overshoot at the centerline as well as in the measuring window. In short, the centerline X_{OH} is affected by the initial transients required to establish a steadily propagating edge flame.

In summary, there are three factors governing the degree of OH overshoot: (1) curvature of the leading edge of the flame, (2) curvature of the initial radial flame extent, and (3) the initial transient associated with igniting and establishing a steady edge flame.

4. Nonpremixed flame structure

In the present study, the structure of the steady nonpremixed flame that is established following thermal runaway is of interest because the fuel is heavily diluted with nitrogen such that the fuel concentration is below the flammability limit at a = 300 s^{-1} with ambient fuel and air (note that the lean limit is $X_{H2} \approx 0.15$ at a = 300 s^{-1} and T_2 = 298 K). As a result, the flame in this study may be sustained by the additional enthalpy from the heated oxidizer stream. The location and structure of this flame is discussed in this section.

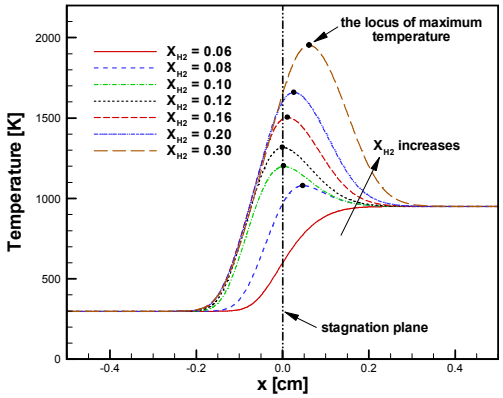

Figure 8: Temperature profiles of one-dimensional axisymmetric hydrogen/air nonpremixed counterflow flames. Fuel and heated oxidizer are issued from the left and right, respectively. T_1 = 298 K, T_2 = 950 K, and a = 300 s^{-1}.

It is found that the nonpremixed flame resides in the oxidizer stream although the stoichiometric mixture fraction (Y_{H2}/Y_{O2} = 0.125 or mixture fraction ξ_{st} = 0.8252) resides in the fuel stream. Accounting for the Lewis number effect on the stoichiometry [20], the modified stoichiometry ($Le_{O2}Y_{H2}/Le_{H2}Y_{O2}$ = 0.0375, where Le_{H2} = 0.3 and Le_{O2} = 1.0 are used) still remains in the fuel side. In reality, however, the flame exists on the oxidizer side. To examine why the flame resides in the oxidizer stream, we simulated a hydrogen/air nonpremixed flame in a one-dimensional axisymmetric counterflow configuration for different fuel concentrations using the OPPDIF code [36]. For hydrogen/air nonpremixed flames with ambient oxidizer, the flame location is expected to move towards the oxidizer stream as the fuel concentration increases under constant strain rate. For flames with heated oxidizer, however, we observe a non-monotonic shift in the flame location with increasing fuel concentration.

The temperature profiles of hydrogen/air nonpremixed counterflow flames are presented in Fig. 8 over a range of fuel mole fractions between 0.06 to 0.30. The fuel and oxidizer temperatures are specified as 298 K and 950 K respectively, and the strain rate is 300 s^{-1}. In Fig. 8, note that as X_{H2} increases from 0.08 to 0.12, the flame location, denoted by the maximum temperature, moves toward the stagnation plane. However, for X_{H2} larger than 0.16, the flame location shifts from the stagnation plane towards the oxidizer side again. Note that the flammability limit of the mixture is $X_{H2} \approx 0.071$ at a = 300 s^{-1} and T_2 = 950 K so that for the present case of X_{H2} = 0.08, the mixture is close to the limit. The dependence of the flame structure on increasing amounts of fuel concentration is shown in Fig. 9. Clearly, for X_{H2} = 0.08, O_2 leakage is significant through the flame compared to the richer cases. Moreover, the flame resides far from the stoichiometric position so that the flame location can not be solely determined even with the modified stoichiometry described above. These flame characteristics suggest that the X_{H2} = 0.08 flame is in Liñán's 'premixed flame regime' [2] where one reactant leaks through the reaction zone and the flame characteristics are determined by a given flame temperature or flame location along with boundary conditions like in a premixed flame. For cases with oxidizer leakage, the flames can reside in the fuel lean side of the mixing layer (see Fig. 1 in Ref. [2]).

For heuristic argument purposes, a schematic of the temperature for Liñán's three different diffusion flame regimes [2] is shown in Fig. 10, where the same notation and symbols are used as in Ref. [2]. When the Lewis number of the reactants is unity, one can draw a simple

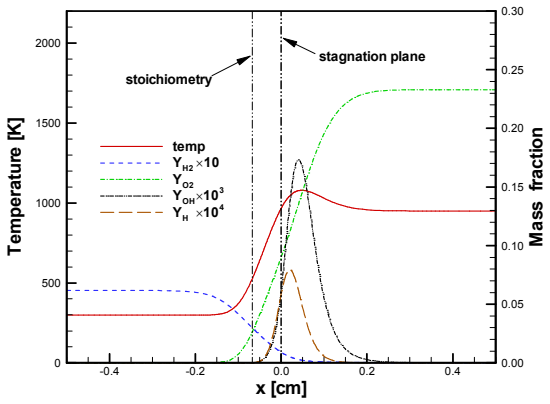

(a) X_{H2} = 0.08

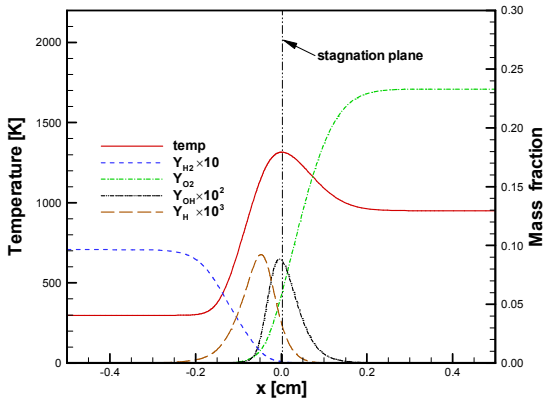

(b) X_{H2} = 0.12

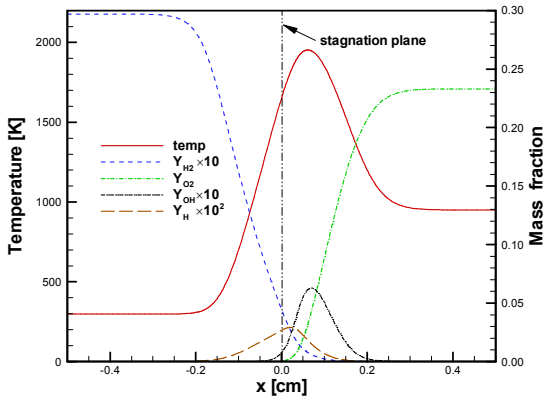

(c) X_{H2} = 0.30

Figure 9: Flame structure for (a) X_{H2} = 0.08, (b) X_{H2} = 0.12 and (c) X_{H2} = 0.30 corresponding to T_1 = 298 K, T_2 = 950 K, and a = 300 s^{-1}.

asymptotic temperature as shown in Fig. 10(a) [2]. However, for cases with fuel Lewis number less than unity, one can not make such a simple asymptotic profile because the Lewis number should be accounted for in the solution of both the energy and species equations. Instead of solving a set of ordinary differential equations, a simple heuristic explanation of the Lewis number effect is described as follows.

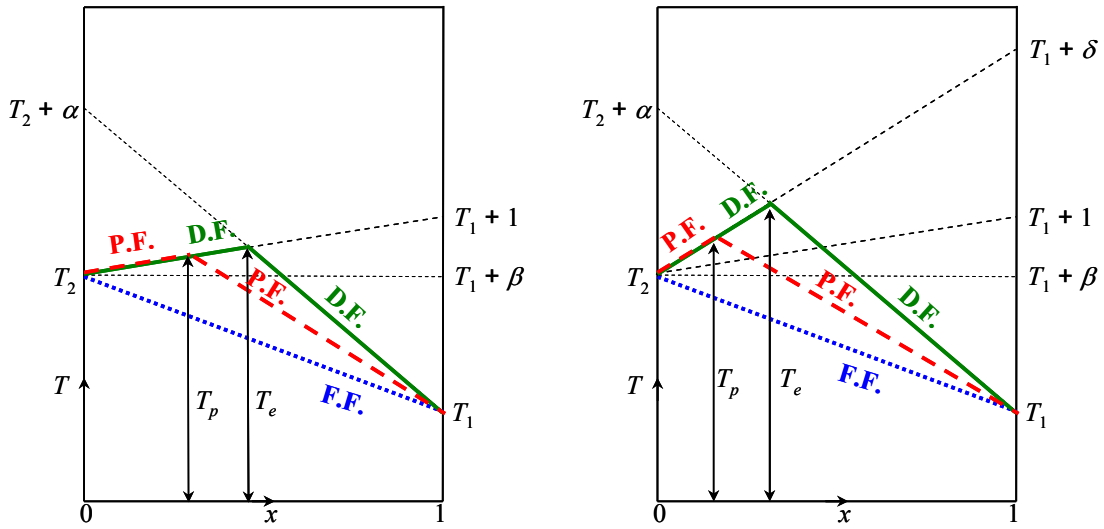

Figure 10: Temperature schematic for frozen flow (F.F.), premixed flame (P.F.), and diffusion flame (D.F.) regimes in the strained coordinated x with $\beta > 0.5$ for (a) reactant Lewis number equal to unity, and (b) fuel Lewis number less than unity. Temperature, T is normalized by the characteristic temperature, $QY_{F,1}/C_p$, and the fuel and oxidizer are normalized by $Y_{F,1}$ and $\nu Y_{F,1}$ respectively, where Q is the heat release rate per unit mass of fuel, ν the stoichiometric mass ratio of oxidizer to fuel, and C_p the specific heat. $\alpha = Y_{O,2}/\nu Y_{F,1}$ and $\beta = (T_2 - T_1)\, C_p / QY_{F,1}$.

For fuel Lewis number less than unity, preferential diffusion of fuel to the flame results in higher reaction rates than for unity Lewis number reactants. Therefore, one can draw an imaginary line 'T_2'–'$T_1 + \delta$' as in Fig. 10(b), which represents the modified $Y_F = 0$ line. From the point of view of the flame, the fuel mass fraction at the fuel stream would be larger than unity so that δ represents the fuel mass fraction at the fuel stream as seen by the flame. With such a modified fuel mass fraction at the fuel stream, one can draw a new temperature profile given in Fig. 10(b). The diffusion flame can attain a higher temperature and the flame location moves further towards the oxidizer side compared to the unity Lewis number case. Similarly, the premixed flame can also have a higher flame temperature and reside further towards the fuel lean side. This provides a heuristic explanation for the Lewis number effect on the flame location accounting for why a $X_{H2} = 0.08$ flame with an effective Lewis number of 0.3 may reside in the fuel lean side. Note that the location and temperature of the diffusion flame can be determined by numerically solving the asymptotic equations [37].

In the 'premixed regime', however, it is known that fast-time instabilities may occur for sub-adiabatic flames with heat loss to the equilibrium side regardless of the amount of heat loss [38]. However, it has also been reported that flames in this regime can be sustained by the stabilizing effect of Lewis number less than unity and/or with a small heat loss parameter [39–41]. In the context of stability, the existence of a flame with $X_{H2} = 0.08$ in the present study confirms the results of the previous asymptotic studies [38–41]. In other words, even though the flame is in the premixed regime, it remains stable because the Lewis number of diluted hydrogen is less than unity and the heat loss to the equilibrium side or the heated oxidizer side is relatively small.

5. The topology of the edge flame

In addition to the location and structure of the nonpremixed flames described above, the topology of the edge flame during ignition is of interest. In general, edge flames in counterflow are straight in the radial direction even though they can have mono-, bi-, and tri-brachial reaction branches at the leading part [19, 42]. However, in both experiments and computations, we observed edge flames that are curved toward the heated oxidizer side as shown in Fig. 2. Similar curved edge flame topology was also reported in a premixture versus heated inert gas in counterflow [18].

The source of the curved topology associated with the edge flame can be determined by examining the local maximum of the adiabatic flame temperature in the axial flow direction. Isocontours of temperature, X_{OH}, and X_{HO2} at 4.5 and 7.5 ms for Case 2 are shown in Fig. 11, where the local maximum of the adiabatic flame temperature along the axial direction is superimposed in the figure. The adiabatic flame temperature, a measure of the sum of the local

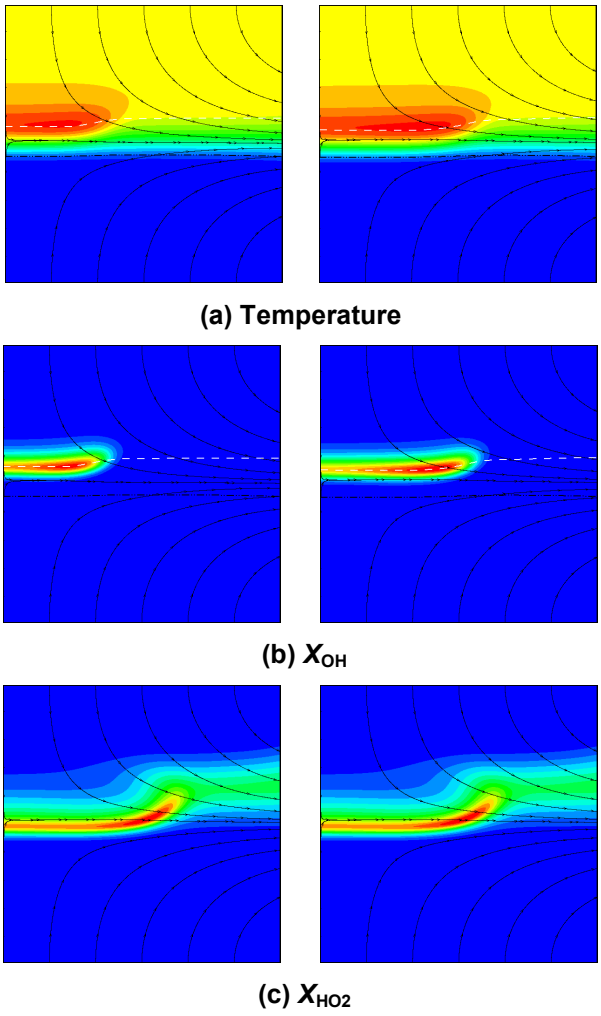

(a) Temperature

(b) X_{OH}

(c) X_{HO2}

Figure 11: Isocontours of temperature, X_{OH}, and X_{HO2} at t = 4.5 (left) and 7.5ms (right) for Case 2. The white dashed line represents the local maximum of the adiabatic flame temperature and arrowed lines correspond to streamlines.

temperature and chemical potential of the mixture, is obtained using the EQUIL code [43] based on local species mass fraction and temperature. Note that in most nonpremixed counterflow flames with ambient fuel and oxidizer, the position of the maximum adiabatic temperature depends primarily on the local mixture composition because the chemical potential of the unburnt mixture is much larger than the local temperature. Thus, it coincides with the stoichiometric position and the corresponding edge flame exhibits a straight flame topology. For the present case, however, the local temperature is comparable to the local chemical potential of the mixture due to the high levels of nitrogen dilution and high temperature of the oxidizer. From Fig. 11, thus, one can observe that the locus of maximum adiabatic temperature lies in the oxidizer stream upstream of the edge flame but exists in the flame near the stagnation plane downstream of the edge flame. The edge flame follows the mixture that has the highest energy and thus, is curved toward the heated oxidizer.

In the context of chemical kinetics, the curved flame topology suggests that the initiation reaction responsible for igniting the edge flame favors the higher temperature of the oxidizer stream, whereas subsequent reactions associated with a steadily propagating edge flame occur under richer conditions, and hence, the flame shifts towards the stagnation plane. As a result of the shift in governing parameter in the reactions, the edge flame shape is curved. A reaction flux analysis shows that, both downstream and upstream of the leading edge, $H + O_2 \rightarrow OH + O$ (R1), $O + H_2 \rightarrow OH + H$ (R2), $OH + H_2 \rightarrow H + H_2O$ (R3), and $H + O_2 + M \rightarrow HO_2 + M$ (R9) are found to be the dominant chain branching and chain termination reactions. In the downstream portion of the edge flame, the temperature is high enough to sustain reactions such that the chain system (R1~R3) favors the fuel rich side for the production of radicals. However, upstream of the edge, the overall reaction favors the high temperature region even though the corresponding mixture becomes leaner at that location. This is because the key chain branching step, R1 is strongly endothermic and thus the chain system (R1~R3) does not proceed in the low temperature region [27, 44]. As a result, HO_2 generated by R9, which maintains the reaction balance with the chain system, is observed in the high temperature region upstream of the edge flame as shown in Fig. 11(c). In summary, the mixture located toward the heated oxidizer stream not only has the highest energy, but also provides a favorable condition for ignition, and hence, the edge flame is curved toward the heated oxidizer side.

The edge flames considered thus far exist in axisymmetric counterflow and propagate in a flow with a radial velocity. Thus, it is conceivable that the edge flame shape is affected by the flow. To understand the contribution of flow variation to the edge flame topology, we investigated edge flames propagating in a quiescent flow in two-dimensional planar counterflow as in Refs. [16–18]. Readers are referred to Appendix A for the problem formulation and results. In summary, the analysis shows that an edge flame topology similar to the experiments [9] is found with sufficiently large Damköhler number. Thus, it is apparent that the curved edge shape is mainly attributed to the aforementioned ignition characteristics and not to flow effects. However, since the model assumes constant density, there still exists the possibility that flow divergence due to heat release may contribute to the asymmetry in the edge topology. In addition, it is also found that near the extinction limit, flame instability occurs and thus, flame strings can be observed as shown in previous studies [19–20].

6. Concluding remarks

The sensitivity of super-equilibrium OH to the initial width and amplitude of the O-atom deposition has been investigated using DNS in a two-dimensional axisymmetric counterflow configuration. The simulations show that the spatial distribution and the magnitude of the OH overshoot are governed by multi-dimensional effects. The degree of OH overshoot increases as the diameter of the initial O-atom deposition region decreases. This result is attributed to preferential diffusion of hydrogen in the highly curved leading portion of the edge flame leading to enhanced reaction rates. As expected, the ignition delay decreases as the amplitude of the initial O-atom deposition increases. For the diluted hydrogen mixture, it is found that the structure of the resulting diffusion flame corresponds to Liñán's 'premixed flame regime' and thus, the flame resides towards the heated oxidizer stream. The curved topology of the edge flame structure resulting from thermal runaway in the nonpremixed counterflow configuration is mainly attributed to the preference of the ignition front for high temperature regions.

Acknowledgments

This work was supported by Sandia National Laboratories, the U. S. Department of Energy, Office of Basic Energy Sciences, Division of Chemical Sciences, Geosciences, and Biosciences and the U. S. Department of Energy SciDAC Program. Sandia National Laboratories is a multiprogram laboratory operated by Sandia Corporation, a Lockheed Martin Company, for the United States Department of Energy under contract DE-AC04-94AL85000.

References

[1] A. Liñán, F. A. Williams, *Combustion and Flame* 120 (1993) 31–46.
[2] A. Liñán, Acta Astronautica 1 (1974) 1007–1039.
[3] C. K. Law, *Combustion and Flame* 24 (1975) 89–98.
[4] A. Liñán, A. Crespo, Combustion Science and Technology 14 (1976) 95–117.
[5] C. G. Fotache, T. G. Kreutz, C. K. Law, *Combustion and Flame* 110 (1997) 429–440.
[6] Y. Tan, C. G. Fotache, C. K. Law, *Combustion and Flame* 119 (1999) 346–355.
[7] C. G. Fotache, Y. Tan, C. J. Sung, C. K. Law, *Combustion and Flame* 120 (2000) 417–426.
[8] X. L. Zheng, C. K. Law, *Combustion and Flame* 136 (2004) 168–179.
[9] R. Seiser, J. H. Frank, S. Liu, J. H. Chen, R. J. Sigurdsson, K. Seshadri, *Proceedings of the Combustion Institute* 30 (2005) 423–430.
[10] C. J. Sung, C. K. Law, *Combustion Science and Technology* 129 (1997) 347–370.
[11] H. G. Im, L. L. Raja, R. J. Kee, L. R. Petzold, *Combustion Science and Technology* 158 (2000) 341–363.
[12] S. D. Mason, J. H. Chen, H. G. Im, *Proceedings of the Combustion Institute* 29 (2002) 1628–1636.
[13] E. Mastorakos, T. A. Baritaud, T. J. Poinsot, *Combustion and Flame* 109 (1997) 198–1223.
[14] H. G. Im, J. H. Chen, C. K. Law, *Proceedings of the Combustion Institute* 27 (1998) 1047–1054.
[15] T. Echekki, J. H. Chen, *Combustion and Flame* 134 (2003) 169–191.
[16] J. Daou, A. Liñán, *Combustion Theory and Modelling* 2 (1998) 449–477.
[17] R. W. Thatcher, J. W. Dold, *Combustion Theory and Modelling* 4 (2000) 435–457.
[18] T. G. Vedarjan, J. Buckmaster, *Combustion and Flame* 114 (1998) 267–273.
[19] J. Buckmaster, *Progress in Energy and Combustion Science* 28 (2002) 435–475.
[20] M. Short, J. Buckmaster, S. Kochevets, *Combustion and Flame* 125 (2001) 893–905.
[21] H. G. Im, J. H. Chen, *Combustion and Flame* 119 (1999) 436–454.
[22] H. G. Im, J. H. Chen, *Combustion and Flame* 126 (2001) 1384–1392.
[23] C. S. Yoo, H. G. Im, *Proceedings of the Combustion Insitute* 30 (2005) 349–356.

[24] G. Amantini, J. H. Frank, B. V. Bennett, M. D. Smooke, A. Gomez, "Comprehensive study of extinction, re-ignition, and the evolution of an annular edge flame in a counterflow flame perturbed by vortices," *5th U.S. Combustion Meeting*, San Diego, CA Paper #A04 (2007)
[25] G. Amantini, J. H. Frank, M. D. Smooke, A. Gomez, *Combustion Theory and Modelling* 11 (2007) 47-72.
[26] G. Amantini, J. H. Frank, M. D. Smooke, A. Gomez, *Combustion and Flame* 147 (2006) 133-149.
[27] C. A. Kennedy, M. H. Carpenter, *Applied Numerical Mathematics* 14 (1994) 397–433.
[28] C. A. Kennedy, M. H. Carpenter, R. M. Lewis, *Applied Numerical Mathematics* 35 (2000) 177–264.
[29] K. Mohseni, T. Colonius, *Journal of Computational Physics* 157 (2000) 787–795
[30] J. Li, Z. Zhao, A. Kazakov, F. Dryer, *International Journal of Chemical Kinetics* 36 (2004) 566–575.
[31] R.J. Kee, F.M. Rupley, E. Meeks, J.A. Miller, *CHEMKIN -III: A Fortran Chemical Kinetics Package for the Analysis of Gas-Phase Chemical and Plasma Kinetics*, Sandia Rep. SAND96-8216, Sandia National Laboratories, 1996
[32] K. Seshadri, F. A. Williams, *International Journal of Heat and Mass Transfer* 21 (1978) 251–253.
[33] C. S. Yoo, Y. Wang, A. Troué, H. G. Im, *Combustion Theory and Modelling* 9 (2005) 617–646
[34] C. S. Yoo, H. G. Im, *Combustion Theory and Modelling* 11 (2007) 259–286.
[35] C. S. Yoo, H. G. Im, *Proceedings of the Combustion Insitute* 31 (2007) 701–708.
[36] A. E. Lutz, R. J. Kee, J. F. Grcar, F. M. Rupley, *OPPDIF: A Fortran Program for Computing Opposed–Flow Diffusion Flames*, Sandia. Rep. SAND96-8243, Sandia National Laboratories, 1997.
[37] S. H. Chung, C. K. Law, *Combustion and Flame* 52 (1983) 59–79.
[38] N. Peters, *Combustion and Flame* 33 (1978) 315–318.
[39] J. S. Kim, *Combustion Theory and Modelling* 2 (1998) 273–282.
[40] D. S. Stewart, J. Buckmaster, *SIAM Journal of Applied. Mathematics* 46 (1986) 582–587.
[41] D. Lozinski, J. Buckmaster, *Combustion Science and Technology* 111 (1995) 379–391.
[42] S. H. Chung, *Proceedings of the Combustion Insitute* 31 (2007) 877–892.
[43] R.J. Kee, F.M. Rupley, J.A. Miller, M.E. Coltrin, J.F. Grcar, E. Meeks, H.K. Moffat, A.E. Lutz, G. Dixon-Lewis, M.D. Smooke, J. Warnatz, G.H. Evans, R.S. Larson, R.E. Mitchell, L.R. Petzold, W.C. Reynolds, M. Caracotsios, W.E. Stewart, P. Glarborg, C. Wang, O. Adigun, CHEMKIN Collection, Release 3.6, Reaction Design, Inc., San Diego, CA, 2001.
[44] I. Glassman, *Combustion*, Third Edition, Academic Press, San Diego, CA, 1996.
[45] J. F. Grcar, *The TWOPNT Program for Boundary Value Problems*, Sandia Rep. SAND91–8230, Sandia National Laboratories, 1992.
[46] A. G. Salinger, N. M. Bou-Rabee, R. P. Pawlowski, E. D. Wilkes, E. A. Burrooughs, R. B. Leoucq, L. A. Romero, *LOCA 1.0 Library of Continuation Algorithms: Theory and Implementation Manual*, Sandia Rep. SAND2002-0396, Sandia National Laboratories, 2002.

Appendix A. Edge flames in planar counterflow

To study edge flame propagation in the quiescent flow direction, we investigated one- and two-dimensional flames in planar counterflow by solving a set of energy and species equations with a constant density model [16–20].

A.1. 1-D flame in planar counterflow

Before simulating two-dimensional edge flames, we need to obtain one-dimensional steady solutions to determine the range of Damköhler numbers, *Da*, over which an edge flame can be established. Consider the one-dimensional governing equations in non-dimensional form as in Refs. [17–20]:

$$-x\frac{d}{dx}\begin{pmatrix} T \\ Y_F \\ Y_O \end{pmatrix} = \frac{d^2}{dx^2}\begin{pmatrix} T \\ Y_F / Le_F \\ Y_O / Le_O \end{pmatrix} + DaY_F Y_O e^{-\theta/T}\begin{pmatrix} q \\ -\alpha_F Y_{O,2} \\ -\alpha_O Y_{F,1} \end{pmatrix}. \qquad \text{(A.1)}$$

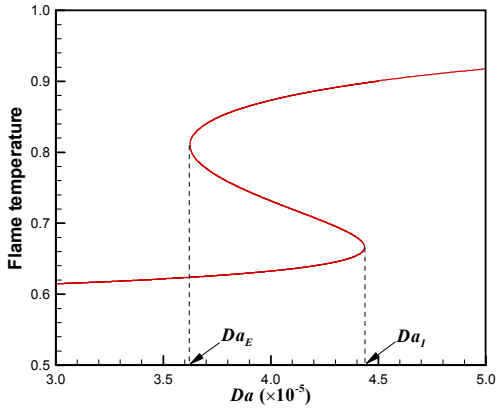

Figure 12: Maximum temperature versus Damköhler number, Da.

The equations are subject to the following boundary conditions:

$$x \to -\infty : T \to T_2,\ Y_F \to 0,\ Y_O \to 1,$$
$$x \to +\infty : T \to T_1,\ Y_F \to 1,\ Y_O \to 0,$$

where Le_F is the fuel Lewis number, Le_O the oxidizer Lewis number, q the heat release rate, θ the activation energy, T_1 the fuel stream temperature, and T_2 the oxidizer stream temperature. In this study, Le_F = 0.3, Le_O = 1.0, q = 0.7, θ = 8.0, T_1 = 0.2, and T_2 = 0.6 were used to emulate the counterflow flames corresponding to a diluted hydrogen mixture counter-flowing against heated oxidizer. Since X_{H2} = 0.08 is considered, $\alpha_F Y_{O,2}$ = 1.0, and $\alpha_O Y_{F,1}$ = 0.2 are specified. In comparison to Short and Buckmaster [20], the fuel mass fraction at the fuel stream, $\alpha_O Y_{F,1}$ and q are decreased, and T_2 is increased.

Figure 12 shows the so-called 'S-curve' of the maximum temperature versus Da obtained from the solution of Eq. (A.1) using the TWOPNT library [45] and continuation algorithms [46]. The extinction Damköhler number, Da_E is found to be 3.625×10^5, and the ignition Damköhler number, Da_I is 4.436×10^5.

A.2. Edge flames in two-dimensional planar counterflow

To investigate edge flame propagation in two-dimensional planar counterflow, the governing equations for one-dimensional counterflow are extended into the z direction and given by:

$$\left(\frac{\partial}{\partial t} - x\frac{\partial}{\partial x}\right)\begin{pmatrix} T \\ Y_F \\ Y_O \end{pmatrix} = \left(\frac{\partial^2}{\partial x^2} + \frac{\partial^2}{\partial z^2}\right)\begin{pmatrix} T \\ Y_F / Le_F \\ Y_O / Le_O \end{pmatrix} + DaY_F Y_O e^{-\theta/T}\begin{pmatrix} q \\ -\alpha_F Y_{O,2} \\ -\alpha_O Y_{F,1} \end{pmatrix}. \qquad \text{(A.2)}$$

Note that there is no flow in the z direction so that edge flame propagation in a quiescent flow can be investigated. To solve Eq. (A.2), S3D was slightly modified such that the fourth-order explicit Runge-Kutta method for time integration and the eighth-order central spatial differencing scheme were used as in the DNS described in the previous sections. The domain size is $L_x \times L_z = 20 \times 40$.

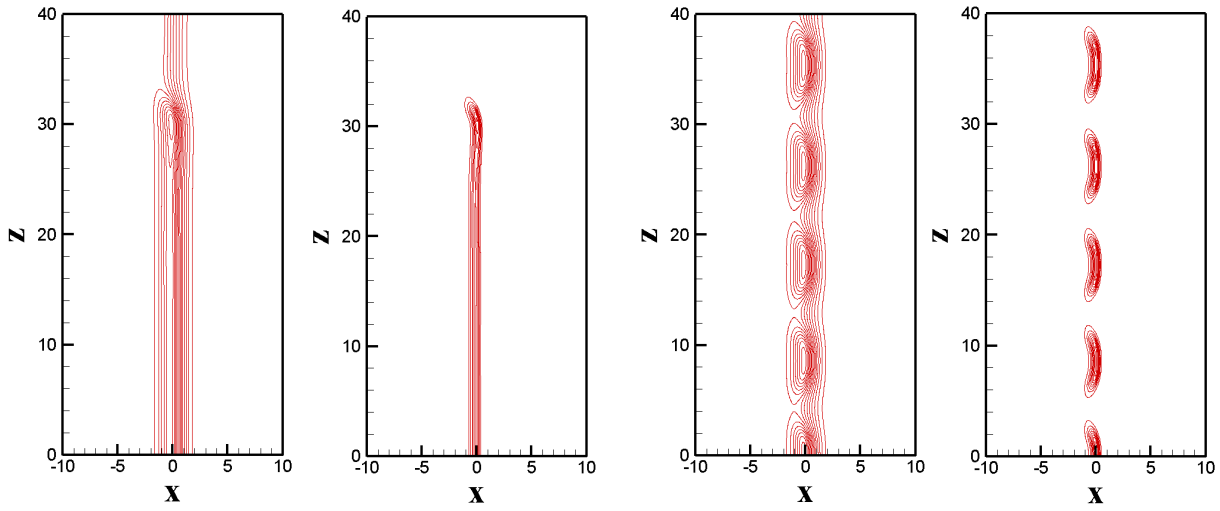

(a) Da = 4.3×10^5 (b) Da = 3.7×10^5

Figure 13: Temperature (left) and heat release (right) isocontours for (a) Da = 4.3×10^5 at t = 30 and (b) Da = 3.7×10^5 at t = 200.

Using two equilibrium solutions with the same *Da* in the upper and lower branches of the S-curve in Fig. 12, an edge flame is established at the center of the domain. Figure 13 presents the temperature and heat release rate for two different Damköhler numbers: (a) $Da = 4.3\times10^5$ at $t = 30$ and (b) $Da = 3.7\times10^5$ at $t = 200$. Two points are to be noted. First, if *Da* is large compared toDa_E, a similar edge flame (ignition front) structure as in the experiments can be observed (see Fig 13(a)). However, as *Da* decreases close to Da_E, flame strings are found as in Ref. [20] (see Fig.13(b)).